

pubs.acs.org/JACS Article

Cylinders-in-Undulating-Lamellae Morphology from ABC Bottlebrush Block Terpolymers

Shuquan Cui, Elizabeth A. Murphy, Wei Zhang, Aristotelis Zografos, Liyang Shen, Frank S. Bates,* and Timothy P. Lodge*



Cite This: J. Am. Chem. Soc. 2024, 146, 6796-6805



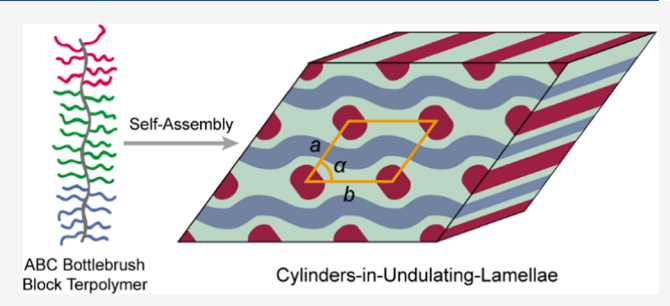
ACCESS

III Metrics & More

Article Recommendations

s Supporting Information

ABSTRACT: Block polymer self-assembly affords a versatile bottom-up strategy to develop materials with the desired properties dictated by specific symmetries and dimensions. Owing to distinct properties compared with linear counterparts, bottlebrush block polymers with side chains densely grafted on a backbone have attracted extensive attention. However, the morphologies found in bottlebrush block polymers so far are limited, and only lamellar and cylindrical ordered phases have been reported in diblock bottlebrushes. The absence of complex morphologies, such as networks, might originate from the intrinsically stiff backbone



architecture. We experimentally investigated the morphologies of nonfrustrated ABC bottlebrush block terpolymers, based on two chemistries, poly(ethylene-alt-propylene)-b-polystyrene-b-poly(DL-lactic acid) (PEP-PS-PLA) and PEP-b-PS-b-poly(ethylene oxide) (PEP-PS-PEO), synthesized by ring-opening metathesis polymerization of norbornene-terminated macromonomers. Structural characterization based on small-angle X-ray scattering and transmission electron microscopy measurements revealed an unprecedented cylinders-in-undulating-lamellae (CUL) morphology with p2 symmetry for both systems. Additionally, automated liquid chromatography was employed to fractionate the PEP-PS-PLA bottlebrush polymer, leading to fractions with a spectrum of morphologies, including the CUL. These findings underscore the significance of macromolecular dispersity in nominally narrow dispersity bottlebrush polymers while demonstrating the power of this fractionation technique.

■ INTRODUCTION

Bottom-up self-assembly of structured materials offers facile and controllable fabrication approaches that can be much more efficient than time-consuming top-down strategies such as lithography. Block polymers, a quintessential class of self-assembling soft materials with nanoscale structure (usually 10–50 nm), find numerous and diverse applications, for example, as thermoplastic elastomers, and as templates for mesoporous ceramics, and microelectronic materials. Exquisitely tunable and high-resolution morphologies, together with simple processing and manageable cost, make block polymers the materials of choice for a growing set of emerging technologies.

Block copolymer self-assembly is driven by a competition between the interfacial tension associated with microphase separated domains and the entropic cost of chain stretching required to fill space uniformly. Linear flexible AB diblock copolymers represent the simplest example, where phase behavior is primarily governed by two parameters: (i) the segregation strength χN , where χ and N denote the Flory–Huggins segment–segment interaction parameter and the degree of polymerization, both defined based on a common segment volume, and (ii) the volume fraction f_A of block A. 12,13 Reducing or increasing f_A from the symmetric condition

 $f_{\rm A}=0.5$ induces interfacial curvature, resulting in the following sequence of phases: one-dimensional (1D) lamellae (LAM), three-dimensional (3D) double gyroid network (GYR), two-dimensional (2D) hexagonally packed cylinders (HEX), 3D ordered spheres (S), and a disordered state (DIS) phase. During the last few decades, more complex molecular architectures such as linear multiblocks and various branched configurations have been synthesized by exploiting modern synthetic methods, enabling a plethora of additional intriguing phases and spawning numerous opportunities for both academic studies and industrial applications. $^{14-16}$

Recently, bottlebrush polymers, with side chains densely grafted on a backbone, have attracted much attention owing to their unique structural and dynamical properties compared with linear counterparts. Crowding of the side chains tends to drive elongated molecular configurations, leading to significantly increased end-to-end chain dimensions. Accord-

Received: December 1, 2023 Revised: January 29, 2024 Accepted: January 31, 2024 Published: February 29, 2024





Scheme 1. Synthesis Route to PEP-PS-PLA and PEP-PS-PEO Bottlebrush Block Terpolymers

ingly, microphase separated block bottlebrushes self-assemble with domain spacings that can reach several hundred nanometers; this is not practical with finite molecular weight coil-like linear block polymers. ^{20,21} Such expanded morphologies are promising for applications such as photonic crystals, which require dimensions approaching the wavelength of visible light.^{22,23} Based on self-consistent field theory (SCFT), Park et al. demonstrated that the GYR phase is thermodynamically stable at compositions between the LAM and HEX phases in bottlebrush diblock copolymer melts.²⁴ However, we hasten to note that these mean-field calculations $(N \to \infty)$ do not faithfully represent the situation at finite molecular weights $(N < \infty)$ due to an inability to account for excluded volume associated with the branched chains; the associated Gaussian coil configurations do not reflect the worm-like behavior of the bottlebrush molecule. In experiments with AB bottlebrush diblocks, only ordered HEX and LAM phases have been found; the complex GYR network state is completely absent. 25,26 Compared with linear polymers, the stiff bottlebrush architecture makes it more difficult to fill space at uniform density throughout the 3D network domains, somewhat analogous to the exclusion of the double diamond and plumber's nightmare network phases in linear conformationally symmetric diblock copolymer melts.²⁷ Extending the block bottlebrushes to more exotic architectures, such as bottlebrushes with Janus blocks, generates a series of nonconventional self-assembly morphologies, as reported in recent works. $^{28-30}$

Recently, we discovered that adding a third bottlebrush block to an AB bottlebrush diblock copolymer opened a window in phase space where the core—shell GYR phase becomes stable.³¹ In this study, we expand on this finding and experimentally investigate ABC bottlebrush block terpolymers satisfying $\chi_{AC} > \chi_{AB} \approx \chi_{BC}$ (referred to as nonfrustrated triblock terpolymers¹⁶), based on two complementary chemistries: poly(ethylene-*alt*-propylene)-*b*-polystyrene-*b*-poly(DL-lactic acid) (PEP-PS-PLA) and PEP-*b*-PS-*b*-poly(ethylene oxide) (PEP-PS-PEO) (Scheme 1), synthesized by graft-through ring-opening metathesis polymerization (ROMP). An unprecedented morphology, cylinders-in-undulating-lamellae (CUL), with *p*2 symmetry, was achieved over a substantial range of PS-

rich compositions. Strikingly, the CUL phase occurs across a similar range of compositions where the orthorhombic *Fddd* single network (O⁷⁰) structure has been reported in linear PI-PS-PEO triblock terpolymers, where PI is 1,4-poly-(isoprene). This study demonstrates that the stiff bottlebrush architecture provides new opportunities for the development of materials with attractive morphologies.

RESULTS

Polymer Synthesis and Characterization. ABC triblock bottlebrush terpolymers (PEP-PS-PLA and PEP-PS-PEO) were prepared by sequential ROMP of norbornene-functionalized macromonomers, PEP (MM_P), PS (MM_S), and PLA (MM_A) or PEO (MM_O), with the Grubbs third generation catalyst based on methods described in the literature³¹ and shown in Scheme 1. A series of child ABC bottlebrush triblock terpolymers along the isopleth with constant $f_{\rm PEP}/f_{\rm PS}$ in the ternary phase portrait was efficiently synthesized by extending a parent AB bottlebrush diblock copolymer with a C block. Specific details regarding polymer synthesis and characterizations can be found in Table 1 and the Supporting Information (Scheme S1, Figures S1-S5, and Tables S1-S2). The molecular weight of all macromonomers was around 1-2 kg/mol, leading to approximately symmetric bottlebrush architectures with persistence length $l_p \approx R_{\rm sc} \approx 1$ nm (see the Supporting Information for detailed calculation), where R_{sc} is the side-chain radius of gyration. All of the bottlebrushes satisfy $l_g < 2R_{sc}$, where $l_g = 0.62$ nm denotes the distance between two neighboring grafting sites, producing extended, worm-like conformations.³⁴ For convenience, the ABC bottlebrush terpolymers are identified as $A_{N_{bb}(A)}^{f_A}$ - $B_{N_{bb}(B)}^{f_B}$ - $C_{N_{bb}(C)}^{f_C}$, where the superscripts and the subscripts denote the volume fraction f and the backbone degree of polymerization $N_{\rm bb}$ of the indicated blocks, respectively.

Identification of CUL Morphology in PEP-PS-PLA Bottlebrush Terpolymers. Bulk morphologies of the ABC bottlebrush block terpolymers were characterized by combining reciprocal space (i.e., small-angle X-ray scattering, SAXS) and real space (i.e., transmission electron microscopy, TEM and electron tomography, ET) characterization techniques. Dried polymers were annealed well above the glass-transition

Table 1. Molecular Parameters of the Synthesized **Bottlebrush Block Polymers**

${ m ID}^a$	$f_{\rm A}^{b}$	$f_{\rm B}^{b}$	$f_{\rm C}^{^{^{}}}$	$M_{\rm n} ({\rm kg/mol})^c$	D^d
PEP _{9.0} ^{0.56} -PS _{9.0} ^{0.44} -PLA _{0.0} ^{0.00}	0.56	0.44	0.00	22.8	1.12
$PEP_{9.0}^{0.47}$ - $PS_{9.0}^{0.37}$ - $PLA_{3.3}^{0.16}$	0.47	0.37	0.16	28.6	1.13
$PEP_{9.0}^{0.45}$ - $PS_{9.0}^{0.35}$ - $PLA_{4.1}^{0.20}$	0.45	0.35	0.20	30.1	1.13
$PEP_{8.4}^{0.50}$ - $PS_{10.6}^{0.50}$ - $PLA_{0.0}^{0.00}$	0.50	0.50	0.00	23.9	1.12
$PEP_{8.4}^{0.43}\text{-}PS_{10.6}^{0.43}\text{-}PLA_{2.8}^{0.14}$	0.43	0.43	0.14	29.0	1.14
PEP _{8.4} ^{0.40} -PS _{10.6} ^{0.39} -PLA _{4.6} ^{0.21}	0.40	0.39	0.21	32.1	1.13
PEP _{8.4} -PS _{10.6} -PLA _{6.0} ^{0.25}	0.38	0.37	0.25	34.7	1.14
$PEP_{8.4}^{0.32}\text{-}PS_{10.6}^{0.32}\text{-}PLA_{10.0}^{0.36}$	0.32	0.32	0.36	41.8	1.15
$PEP_{8.4}^{0.46}-PS_{12.4}^{0.54}-PLA_{0.0}^{0.00}$	0.46	0.54	0.00	26.3	1.12
$PEP_{8.4}^{0.39}$ - $PS_{12.4}^{0.45}$ - $PLA_{3.6}^{0.16}$	0.39	0.45	0.16	32.7	1.14
PEP _{8.4} ^{0.37} -PS _{12.4} ^{0.43} -PLA _{4.7} ^{0.20}	0.37	0.43	0.20	34.7	1.14
$PEP_{8.4}^{0.36}$ - $PS_{12.4}^{0.41}$ - $PLA_{5.9}^{0.23}$	0.36	0.41	0.23	36.8	1.15
$PEP_{6.6}^{0.39}-PS_{13.4}^{0.61}-PLA_{0.0}^{0.00}$	0.39	0.61	0.00	25.1	1.12
PEP _{6.6} ^{0.36} -PS _{13.4} ^{0.57} -PLA _{1.4} ^{0.07}	0.36	0.57	0.07	27.6	1.12
$PEP_{6.6}^{0.33}-PS_{13.4}^{0.52}-PLA_{3.3}^{0.15}$	0.33	0.52	0.15	31.0	1.13
PEP _{6.6} ^{0.31} -PS _{13.4} ^{0.49} -PLA _{4.7} ^{0.20}	0.31	0.49	0.20	33.4	1.13
$PEP_{6.6}^{0.30}$ - $PS_{13.4}^{0.47}$ - $PLA_{5.5}^{0.23}$	0.30	0.47	0.23	34.9	1.14
PEP _{6.6} ^{0.28} -PS _{13.4} ^{0.44} -PLA _{7.2} ^{0.29}	0.28	0.44	0.29	38.0	1.15
PEP _{6.6} ^{0.24} -PS _{13.4} ^{0.38} -PLA _{11.1} ^{0.38}	0.24	0.38	0.38	44.8	1.17
$PEP_{9.7}^{0.39}-PS_{19.0}^{0.61}-PLA_{0.0}^{0.00}$	0.39	0.61	0.00	36.1	1.12
PEP _{9.7} ^{0.32} -PS _{19.0} ^{0.49} -PLA _{6.2} ^{0.19}	0.32	0.49	0.19	47.1	1.15
PEP _{5.6} ^{0.39} -PS _{11.3} ^{0.61} -PLA _{0.0} ^{0.00}	0.39	0.61	0.00	21.3	1.12
PEP _{5.6} ^{0.33} -PS _{11.3} ^{0.53} -PLA _{2.5} ^{0.14}	0.33	0.53	0.14	25.7	1.13
PEP ^{0.38} _{7.3} -PS ^{0.62} _{15.4} -PLA ^{0.00} _{0.0}	0.38	0.62	0.00	28.6	1.13
PEP ^{0.32} _{7.3} -PS ^{0.52} _{15.4} -PLA ^{0.16} _{3.9}	0.32	0.52	0.16	35.5	1.14
$PEP_{6.4}^{0.33}-PS_{16.7}^{0.67}-PLA_{0.0}^{0.00}$	0.33	0.67	0.00	29.1	1.12
PEP ^{0.29} _{6.4} -PS ^{0.58} _{16.7} -PLA ^{0.13} _{3.1}	0.29	0.58	0.13	34.6	1.15
$PEP_{6.4}^{0.27}$ - $PS_{16.7}^{0.54}$ - $PLA_{5.0}^{0.19}$	0.27	0.54	0.19	37.9	1.15
$PEP_{6.4}^{0.25}-PS_{16.7}^{0.51}-PLA_{6.8}^{0.25}$	0.25	0.51	0.25	41.1	1.16
$PEP_{16.9}^{0.41}-PS_{30.8}^{0.59}-PLA_{0.0}^{0.00}$	0.41	0.59	0.00	59.9	1.12
$PEP_{16.9}^{0.38}\text{-}PS_{30.8}^{0.54}\text{-}PLA_{6.2}^{0.09}$	0.38	0.54	0.09	66.7	1.16
					4

^aSamples with the same parent diblock identified as $A_{N_{bb}(A)}^{f_{A}}$ - $B_{N_{bb}(B)}^{f_{B}}$ - $C_{N_{bb}(C)}^{f_C}$, where N_{bb} was calculated using the volume fraction f and the number-average molecular weight M_n . ^bDetermined by proton nuclear magnetic resonance (¹H NMR) spectroscopy with the density of each block $\rho_{\rm PEP}$ = 0.79 g/mL, $\rho_{\rm PS}$ = 0.969 g/mL, $\rho_{\rm PLA}$ = 1.154 g/mL, and $\rho_{\rm PEO}$ = 1.064 g/mL. 32,35,36 CThe $M_{\rm n}$ of diblocks was determined by size-exclusion chromatography (SEC) with a multiangle laser light scattering (MALS) detector as well as a refractive index (RI) detector using tetrahydrofuran (THF) as the mobile phase. The M_n of triblocks was calculated by combining the M_n of the parent diblock and the weight fraction of each block. ^dDetermined by SEC with an RI detector using THF as the eluent.

temperature $T_{\rm g}$ and the melting temperature $T_{\rm m}$ (if present) of all blocks (Figures S6-S7), usually at 150 °C under vacuum for 24 h. Size-exclusion chromatography (SEC) profiles in Figure S5 confirmed that neither cross-linking nor degradation occurred during such annealing. We conducted the SAXS experiments above T_m to avoid artifacts, such as breakout crystallization of the PEO, which could disrupt the melt state morphology. For consistency, the measurements on PEP-PS-PLA were also conducted at elevated temperatures. Specifically, the annealed samples were mostly measured usually at 140 °C, supplemented by several measurements at 80 °C for specimens that were close to the order-disorder transition at 140 °C due to relatively low molecular weight. None of the bottlebrush polymers exhibited an order-order transition between 80 and 140 °C, although some samples with

coexisting phases became single-phase at higher temperatures (190 °C). SAXS experiments were carried out either at the Advanced Photon Source (APS) at Argonne National Laboratory, Sector 5-ID-D beamline (X-ray wavelength λ = 0.0729 nm) or using a Xenocs Ganesha instrument ($\lambda = 0.154$ nm) equipped with a four-position INSTEC heating stage at the College of Science & Engineering Characterization Facility, University of Minnesota. TEM images were collected on an FEI Tecnai Spirit Bio-Twin TEM with an accelerating voltage of 120 kV. Ultrathin sections (~70 nm) were prepared for TEM analysis by cryo-microtoming the annealed ABC bottlebrush samples at around -70 °C. Thin sections were then transferred to 400-mesh copper grids, followed by RuO₄ vapor staining for 3-5 min to enhance the contrast.

An intriguing morphology was uncovered in a subset of ABC bottlebrush block terpolymers. Figure 1 provides a representative azimuthally integrated synchrotron SAXS pattern (the 2D SAXS pattern is shown in Figure S8) and a typical TEM image from the sample PEP_{6,6}^{0.33}-PS_{13,4}^{0.52}-PLA_{3,3}^{0.15}. Bragg peaks are located at q values consistent with 2D plane group p2, where the scattering wavevector is given by $q = 4\pi\lambda^{-1}\sin(\theta/2)$ in which θ is the scattering angle. Indexing this SAXS pattern yields unit cell parameters a = 17.1 nm, b = 19.6 nm, and $\alpha = 54.9^{\circ}$. In the PEP-PS-PLA samples, the PS domains are preferentially stained by RuO₄, resulting in white dots alternating with a pattern of undulating lines embedded in a black matrix in the TEM image (Figure 1B). As described further below, the lightly stained dots and lines correspond to PLA and PEP domains, respectively, and the matrix is PS. A unit cell is identified in Figure 1B by a yellow parallelogram with unit cell parameters $a = 17.2 \pm 0.8$ nm, $b = 19.0 \pm 0.9$ nm, and $\alpha = 68.2$ \pm 3.5° (averaged over 20 unit cells). The a and b parameters are consistent with the SAXS-determined dimensions, while the angle α obtained from the TEM images deviates from the SAXS result by 10-20°. We have concluded that this angle deviation reflects either thin sections sliced at an oblique angle or shear deformation during sample preparation and, most probably, a combination of both factors. This type of distorted image has been reported previously by our group, notably in a study of the tetrahedral Frank-Kasper σ -phase.³⁷ Morphological characterization of other PEP-PS-PLA samples are provided in Figures S9-S12, with unit cell parameters (calculated from SAXS) listed in Table S3.

In order to definitively assign a 3D morphology to the structure associated with the results shown in Figure 1, we expanded the TEM analysis through the use of electron tomography (ET), a technique that retrieves structural information from a tilt series of 2D projections.³⁸ A tilt series of TEM-ET images was obtained from a RuO₄-stained section of sample $PEP_{6.6}^{0.31}$ - $PS_{13.4}^{0.49}$ - $PLA_{4.7}^{0.20}$ using an FEI TF30 field emission gun transmission electron microscope with an accelerating voltage of 300 kV. The 3D reconstruction was carried out with IMOD, 39 followed by a subtomogram averaging procedure using Dynamo. 40 Specific details of the experiment and image reconstruction are provided in the Supporting Information. The reconstruction map (surface style) is shown in Figure 2, and Video S1 elucidates a clear cylinders-in-undulating-lamellae morphology, where the cylinders and the undulating lamellae correspond to the dots and the undulating lines observed in the single projected 2D TEM image (Figure 1B), respectively. Defects at the edge of the map are attributed to the low edge contrast (Figure S13) caused by the limitation of the reconstruction algorithm and the limited

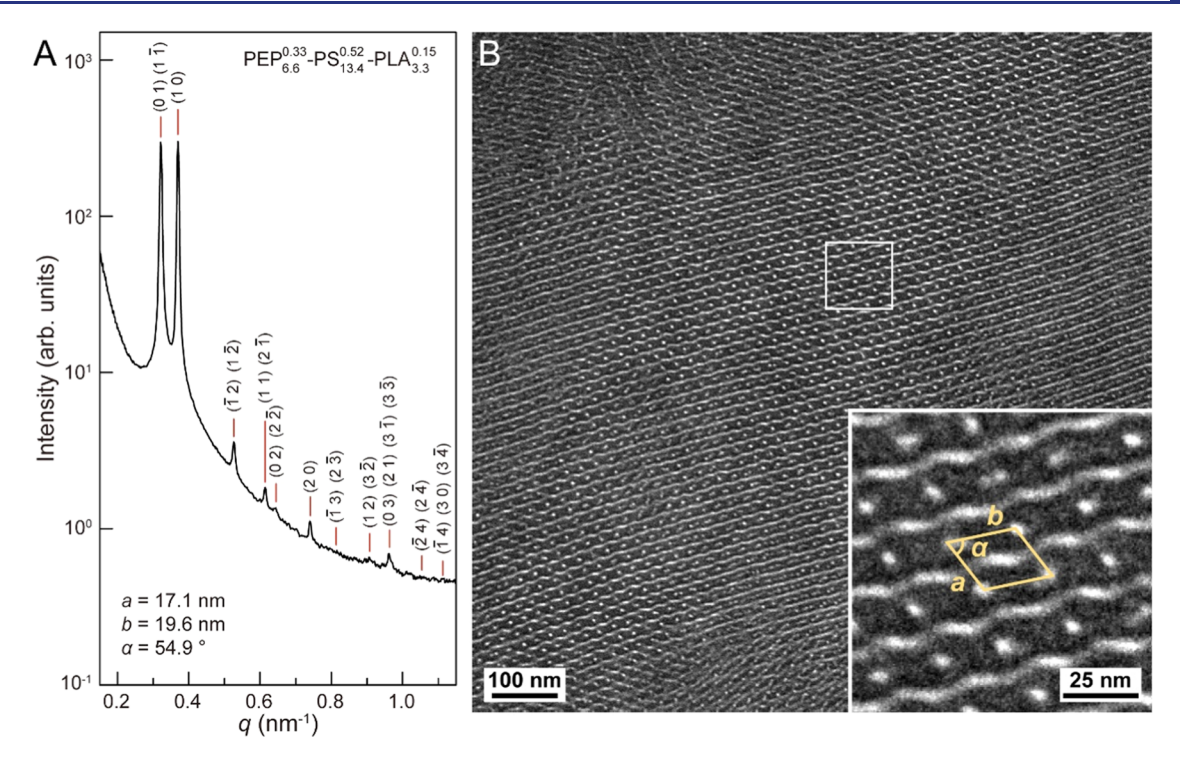


Figure 1. (A) Synchrotron SAXS pattern measured at 140 °C and (B) TEM image from sample $PEP_{6.6}^{0.33}-PS_{13.4}^{0.15}-PLA_{3.1}^{0.15}$. The SAXS pattern is indexed with a 2D p2 plane group, where the indices (h k) are identified by vertical lines. The TEM section in panel (B) was stained with RuO₄, which preferentially reacts with PS. A magnified version of the squared region is inserted at the bottom right, where a unit cell is identified by the yellow parallelogram.

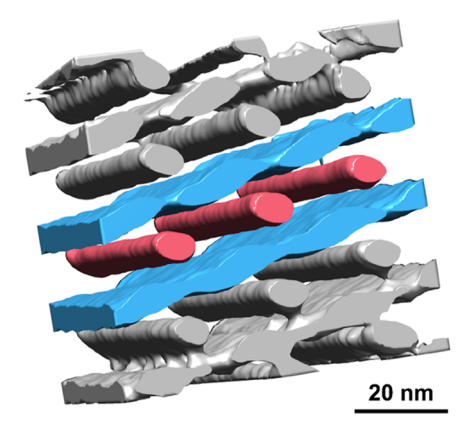


Figure 2. 3D reconstruction map from a RuO₄-stained thin section of PEP $_{6.6}^{0.31}$ -PS $_{13.4}^{0.49}$ PLA $_{4.7}^{0.20}$. A cylinders-in-undulating-lamellae morphology is visualized. The PS region (black domain after staining) has been made transparent; three cylinders and two undulating layers have been colored red and blue, respectively.

subtomograms for averaging. A depiction of the CUL morphology is provided in Figure 3.

CUL Phase in the Ternary Phase Portrait. We further explored the location of the CUL phase in the ternary phase portrait of the ABC bottlebrush triblock terpolymers, as exemplified by PEP-PS-PLA bottlebrushes. Polymer morphologies were mainly determined by SAXS, supplemented by TEM images (representative data are provided in Figures S14–S15). In the expanded phase portrait in Figure 4 (a full-axes phase portrait is presented in Figure S16), the CUL phase occupies a relatively robust PS-rich composition window ($f_{\rm PEP}/f_{\rm PS} < 1$) bounded by 0.24 < $f_{\rm PEP} < 0.44$, 0.39 < $f_{\rm PS} < 0.59$, and 0.13 < $f_{\rm PLA} < 0.29$. Molecular parameters and



Figure 3. Schematical illustration of the CUL phase. A and C blocks fill the blue undulating layers and the red cylinders, respectively, and are embedded in the green B matrix. Sketches of ABC bottlebrush chains show how the morphology is assembled.

morphological information on all samples in the phase portrait are listed in Tables 1 and S2.

In the ternary phase portrait, as the volume fraction of the PEP block gradually increases ($f_{\rm PEP}/f_{\rm PS}>1$), the GYR network appears adjacent to the CUL window. Coexisting GYR and CUL were observed in samples at intermediate compositions ($f_{\rm PEP}/f_{\rm PS}\approx1$). Figure 5 provides the SAXS pattern and TEM image from a typical GYR sample, PEP $_{9.0}^{0.47}$ -PS $_{9.0}^{0.37}$ -PLA $_{3.3}^{0.16}$. Due to the partial staining of the PEP domain and the PLA domain, it is difficult to fully characterize the GYR (e.g., whether it is a core–shell structure) by TEM. We assume it is a core–shell GYR because it occurs at compositions where the core–shell GYR was found in PEP-PS-PEO bottlebrushes, as recently described. ³¹ Data from other samples with the GYR phase can be found in Figures S14–S15.

Identification of CUL Morphology in a PEP-PS-PEO Bottlebrush Terpolymer. A TEM image with another dots-in-undulating-lines pattern was obtained from a PEP-PS-PEO sample (PEP)_{16.9}-PS_{30.8}-PLA_{6.2}^{0.09}), as shown in Figure 6B. Exposing PEP, PS, and PEO to RuO₄ vapor results in unstained, slightly stained, and strongly stained domains,

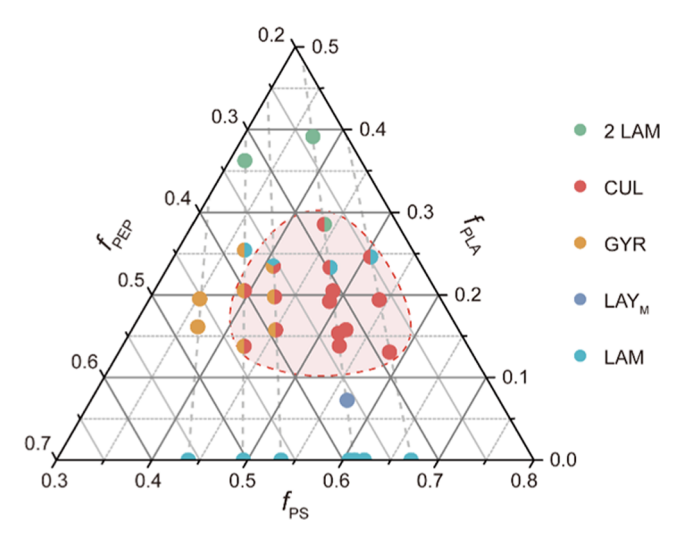


Figure 4. Phase portrait of the PEP-PS-PLA bottlebrush block terpolymers. The CUL phase window is highlighted by the red shadow. Dashed lines indicate isopleths with constant $f_{\rm PEP}/f_{\rm PS}$. LAY_M and 2 LAM denote the modulated layer and two lamellar phases, respectively.

respectively. Accordingly, three domains are distinguishable in the PEP-PS-PEO sample under TEM visualization: black dots (PEO), white undulating lines (PEP), and a gray matrix (PS). A corresponding SAXS pattern is again consistent with p2 symmetry with unit cell parameters a=28.2 nm, b=35.7 nm, and $\alpha=50.7^{\circ}$. Unit cell parameters extracted from 20 places in the TEM image yield $a=28.8\pm1.6$ nm, $b=33.5\pm1.6$ nm, and $\alpha=58.0\pm2.3^{\circ}$, consistent with those determined by SAXS. Compared with the PEP-PS-PLA bottlebrushes, this distinctive morphology occurred at higher molecular weights in the PEP-PS-PEO bottlebrushes ($N_{\rm bb}=53.9$ in PEP-PS-PEO

versus $N_{\rm bb}=19.4-34.9$ in PEP-PS-PLA, Tables 1 and S2); note that $\chi_{\rm PEP-PEO}$ (= 0.157)⁴¹ < $\chi_{\rm PEP-PLA}$ (= 0.437).³⁵ Lower N PEP-PS-PEO samples with $N_{\rm bb}=25-34$ and similar compositions exhibited poorly ordered morphologies, denoted modulated layers (LAY_M),³¹ instead of the well-ordered morphology evident in Figure 6.

Fractionating PEP-PS-PLA Bottlebrush Triblock Terpolymer. Molecular weight distribution or macromolecular dispersity, an intrinsic feature of polymers, plays a role in the phase behavior of block copolymers. 42-45 Bottlebrush block polymers synthesized via ROMP typically exhibit narrow molecular weight distributions, 46,47 a characteristic observed in our polymers as well (θ < 1.2, Figure S5 and Tables 1 and S2). Therefore, the impact of dispersity on the phase behavior is generally not considered a significant concern for bottlebrush polymers. However, previous studies have shown that fractionating a polymer, even with low dispersity, can produce numerous fractions with different compositions and morphologies. 48-51 To scrutinize the dispersity effect on the phase behavior of the bottlebrushes, we fractionated three selected CUL-forming PEP-PS-PLA bottlebrush triblock terpolymers by automated liquid chromatography. It should be noted that ABC triblock terpolymer bottlebrushes exhibit both compositional and molecular weight heterogeneities. Automated chromatography facilitates the separation of polymer chains from an as-synthesized parent polymer based on differential constituent polarity, which enables compositional fractionation. Molecular weight dispersity can be characterized by conventional SEC. The as-synthesized bottlebrush triblock terpolymers were dissolved in dichloromethane and loaded directly onto a commercially available silica gel column (50 g). Suitable elution conditions were identified via thin-layer chromatography (TLC) experiments based on solvent mixtures from 100% hexanes to 100% ethyl acetate (Figure

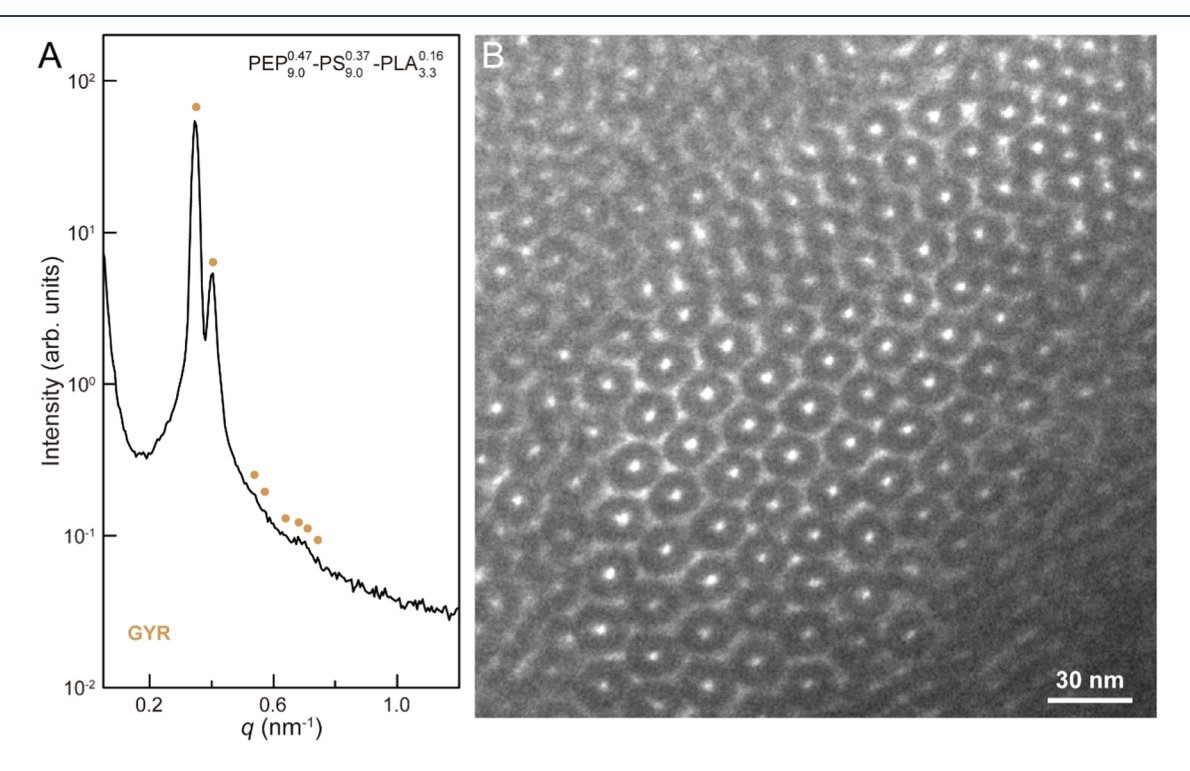


Figure 5. (A) SAXS pattern measured at 140 °C and (B) TEM image from a GYR sample PEP_{9.0}^{0.38}-PS_{9.0}^{0.37}-PLA_{3.3}^{0.16}. The TEM image represents a projection through the (110) gyroid plane.

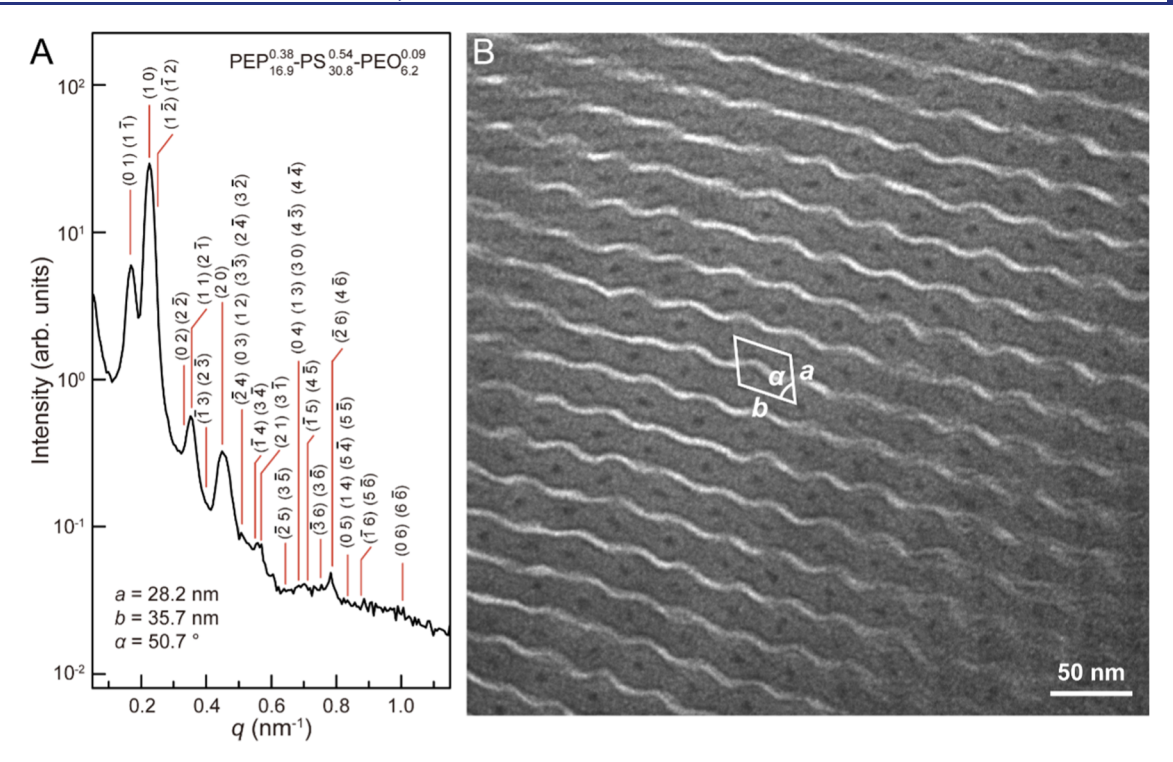


Figure 6. (A) SAXS pattern measured at 140 °C and (B) TEM image obtained from a bottlebrush polymer $PEP_{16.9}^{0.38}-PS_{30.8}^{0.54}-PLA_{6.2}^{0.09}$. A unit cell with p2 symmetry is identified by a white parallelogram.

Table 2. Molecular Parameters of Polymer Fractions and Associated Phases at 80 °C

parent terpolymer	fraction	$f_{\mathtt{PEP}}^{}a}$	$f_{\mathrm{PS}}^{}a}$	$f_{\mathrm{PLA}}{}^{a}$	D^{b}	phase ^c
PEP ^{0.33} -PS ^{0.53} _{11.3} -PLA ^{0.14} _{2.5}	F2	0.30	0.55	0.15	1.31	LAM
	F3	0.35	0.52	0.13	1.12	CUL
	F16-34	0.34	0.64	0.02	1.15	DIS
	F71-116	0.35	0.44	0.21	1.15	CUL

"Determined by ¹H NMR. ^bDetermined by SEC with an RI detector using THF as the eluent. ^cDetermined by SAXS or the combination of SAXS and TEM.

S17). The elution curves and the molecular characterization of the child fractions are provided in Figures S18-S20 and Tables 2 and S4. Our sample nomenclature reflects the sequence of fractions (F, 22 mL for each fraction) collected during separation. Characterization of the resulting libraries by integration of unique ¹H NMR peaks for each block, as well as SAXS and TEM measurements, revealed that the child fractions spanned a broad compositional and morphological window to produce various structures, including CUL, LAM, and DIS, as shown in Figure S21 and listed in Tables 2, S4, and S5. Notably, the CUL was found both in the parent bottlebrush and some of its child fractions. Phase portraits are depicted in Figures 7 and S22-S23. Variation in the phase behavior of the fractions relative to that from the assynthesized parent polymers results from a redistribution of both the molecular weights and compositions (Figures S19-S20 and Tables 2 and S4). For example, the parent bottlebrush $PEP_{5.6}^{0.33}-PS_{11.3}^{0.53}-PLA_{2.5}^{0.14}$ ($f_{PEP}/f_{PS} = 0.62$) and sample F71–116 $(f_{PEP}/f_{PS} = 0.80)$ both exhibit a well-defined CUL morphology, compared to the DIS state of sample F16-34 (Table 2 and Figure 7), which likely reflects a more asymmetric composition ($f_{PEP}/f_{PS} = 0.53$) and minimal PLA content. A size-exclusion-based breakthrough (Figure S18) was observed early in the separation, even when various strategies (dry loading, wet loading, eluent strength, etc.) were used,

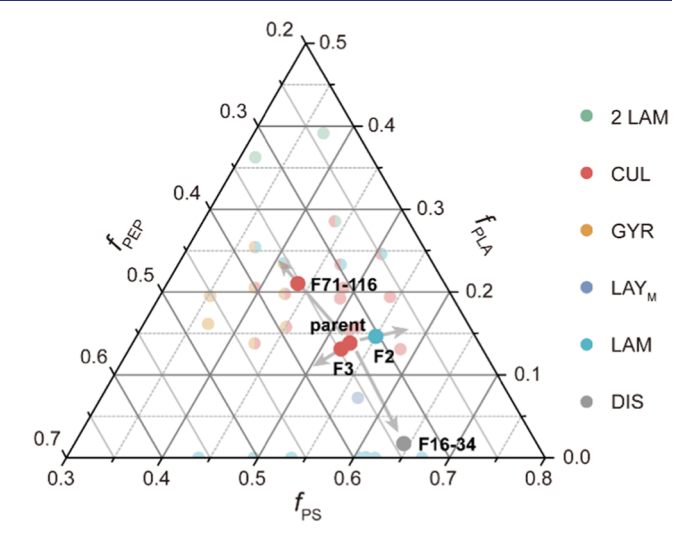


Figure 7. Phase portrait of fractions F2, F3, F16–34, and F71–116 separated from $PEP_{5.6}^{0.33}$ - $PS_{11.3}^{0.53}$ - $PLA_{2.5}^{0.14}$ (parent). The small light-colored circles correspond to synthesized polymers.

which accounts for the high dispersity of early fractions, such as F2 from $PEP_{5.6}^{0.33}$ - $PS_{11.3}^{0.53}$ - $PLA_{2.5}^{0.14}$ (Table 2), whereas latter fractions were successfully fractionated by composition.

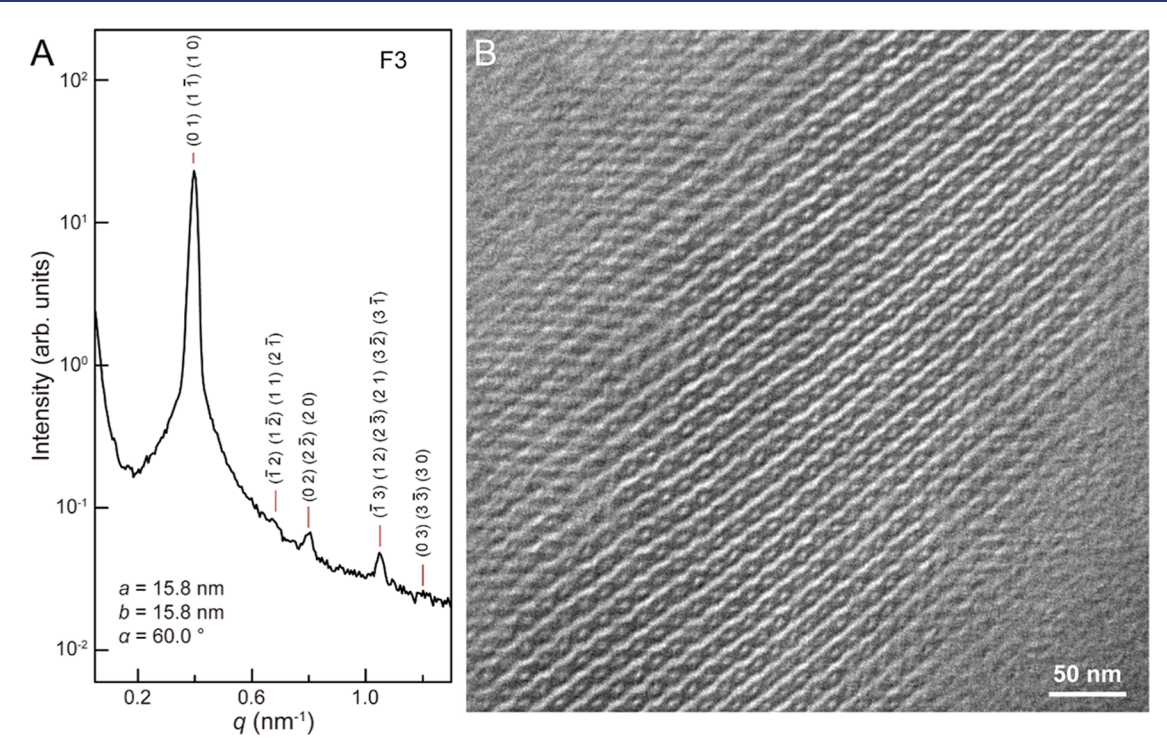


Figure 8. (A) SAXS pattern measured at 80 °C and (B) TEM image from F3 fractionated from PEP $_{5.6}^{0.33}$ -PS $_{11.3}^{0.53}$ -PLA $_{2.5}^{0.14}$. Morphological characterizations suggest a CUL morphology with a=b and $\alpha=60^{\circ}$.

Collectively, these results underscore the utility of automated chromatography to interrogate the effects of composition and dispersity on the phase behavior of complex block polymer materials.

Interestingly, a SAXS pattern with a tentative *p6mm* symmetry appeared in one of the fractions, F3, from PEP $_{5.6}^{0.33}$ -PS $_{11.3}^{0.53}$ -PLA $_{2.5}^{0.14}$ (Figure 8). We utilized TEM to scrutinize the morphology, and the image shown in Figure 8 confirms that this morphology also is a CUL structure. The unit cell parameters satisfy a=b and $\alpha=60^{\circ}$, leading to overlapping of the (01), (10), and (1 $\overline{1}$) Bragg reflection peaks found in Figures 1A and 6A. These results demonstrate the importance of combining both reciprocal space (SAXS) and real space (TEM) characterizations for phase assignment.

DISCUSSION

In this study, we synthesized two types of nonfrustrated ABC bottlebrush block terpolymers, PEP-PS-PLA and PEP-PS-PEO, by ROMP. Morphological investigations based on SAXS, TEM, and ET (Figures 1-2 and 6) identified a CUL morphology with p2 symmetry (Figure 3) in both systems, suggesting the universality of this phase in nonfrustrated ABC bottlebrush block terpolymers. The CUL appears to be thermodynamically stable based on (i) consistent results obtained with thermal annealing and solvent casting (Figure S11) and (ii) thermal reversibility of the CUL phase suggested by temperature-dependent experiments (Figure S12). Systematically scanning the compositional space revealed that this morphology occurred in the PS-rich region $(f_{PEP}/f_{PS} < 1)$, bordering the GYR network window $(f_{PEP}/f_{PS} > 1)$ (Figure 4). The CUL is observed in both the as-synthesized polymers and polymer fractions derived from automated fractionation (Figure 7).

The phase behavior of ABC triblocks is determined by compositions $(f_{\rm A},\ f_{\rm B},\ {\rm and}\ f_{\rm C})$ and the relative interaction

strengths χ_{AC} , χ_{AB} , and χ_{BC} . ^{14,16} ABC triblocks have been classified as nonfrustrated (χ_{AC} is greater than χ_{AB} and χ_{BC}) and frustrated (χ_{AC} is intermediate between χ_{AB} and χ_{BC}) versions. ¹⁶ A similar cylinders-in-lamellae phase has been documented in frustrated linear ABC block terpolymers and polymer blends, such as PS-*b*-polybutadiene-*b*-poly(*tert*-butyl methacrylate) (SBT) ⁵² and blends of PS-*b*-poly(2-vinyl-pyridine) (SV) and partially saponified PS-*b*-poly(1,2-butadiene)-*b*-poly(*tert*-butyl methacrylate) (SB(T/A) with A being poly(methacrylic acid)). ⁵³ The reported packing symmetry of cylinders in these systems was either hexagonal or ill-defined due to inadequate morphological information. In this study, both ABC bottlebrushes are nonfrustrated triblock terpolymers. Specifically, $\chi_{PEP-PLA}$ (= 0.437) ³⁵ > χ_{PEP-PS} (= 0.069) ⁵⁴ $\approx \chi_{PS-PLA}$ (= 0.078) ⁵⁵ and $\chi_{PEP-PEO}$ (= 0.157) ⁴¹ > χ_{PEP-PS} (= 0.069) ⁵⁶ where the values in parentheses denote the χ values at 140 °C. In the nonfrustrated linear counterparts (such as PI-PS-PEO), an *Fddd* single network (O⁷⁰) appears at similar compositions. ^{32,33}

A core-shell GYR was found in both PEP-PS-PLA (Figures 4-5) and PEP-PS-PEO (previous work³¹) bottlebrushes at compositions where this core-shell morphology occurs with linear counterparts.⁵⁷ In contrast, the Fddd network phase disappears in ABC triblock bottlebrushes and is replaced by the non-network CUL. Concurrent disappearance of the Fddd network but survival of the core-shell GYR in bottlebrushes are unexpected. A complicating factor is that self-consistent field theory (SCFT), the principal theoretical tool for rationalizing block polymer phase behavior, is not applicable to highly branched macromolecules at finite molecular weights; the theory simply does not properly account for the associated excluded volume effects. A possible mechanism underlying this phenomenon involves decreased AC contacts resulting from rigid ABC bottlebrush architectures. A published SCFT study by Tyler et al. demonstrated that the *Fddd* phase in ABC linear

terpolymers is a core-shell network analogous to the coreshell GYR: the C domain forms a single 3-fold connected network within the A matrix, while A and C domains are separated by a weakly segregated B-rich shell, which allows limited contact between the A (network) and C (matrix) domains without an actual AC interface. The core-shell Fddd network seems sensitive to the AC contact since the phase window along the $f_A = f_B$ isopleth narrows and quickly closes with increasing $\chi_{\rm AC}$ (decreasing AC contact). The sensitivity to the interaction between the network domain and the matrix domain in the ABC core-shell Fddd structure closely mirrors that in the Fddd network in AB diblocks, surviving only in the weakly segregated region.⁵⁹ In contrast, we speculate that the core-shell GYR is not reliant on AC contact, since this network morphology persists in diblocks as an equilibrium phase in the strong segregation regime.⁵⁷ In comparison to ABC linear terpolymers, the stiffness of the bottlebrush polymers, along with the crowding of side chains around the backbone, must hinder side-chain penetration, thereby screening contact between the A and C domains. This "screening effect" is general in bottlebrush polymers and has been utilized to account for the reduction in $\chi_{\rm eff}$ (= 0.03) in PS-PEO bottlebrushes compared with the corresponding linear polymers (= 0.08). 60 Consequently, we speculate that the CUL phase predominates over the Fddd network in ABC bottlebrush block terpolymers. The CUL phase, a combination of cylinders and lamellae, likely has a total free energy that reflects an intermediate curvature to those of the cylinder and lamellae phases.⁶¹ A more definitive understanding of the phase behavior awaits advances beyond SCFT.

One interesting phenomenon is that the a parameter increases more slowly than the b parameter with increasing $f_{\rm C}$ or $N_{\rm bh}({\rm C})$ values in the CUL samples (Table S3). We speculate that this asymmetric tendency of a and b with composition is due to the limitation of the "neck" (the region between two nearest neighbor cylinders sandwiched by two undulating layers, see Figure 3) in the CUL morphology. ABC terpolymers at the "neck" region have to bend to a relatively large extent; thus, the transverse distance (related to the a parameter) of the "neck" is mainly determined by the first two blocks, PEP and PS. As a result, extension of the C block contributes more to the b value. Moreover, the extended C block enhances the segregation strength (χN) and imparts increased rigidity to the bottlebrush, resulting in a reduction of α . The inherent flexibility in the unit cell parameters of the CUL phase holds significant promise for tailoring its physical properties to meet specific applications such as integrated circuit manufacturing, nanoporous membranes, and advanced optical devices.

CONCLUSIONS

In this study, two nonfrustrated ABC bottlebrush block terpolymers, PEP-PS-PLA and PEP-PS-PEO, were synthesized by ROMP. Morphological characterization based on SAXS, TEM, and ET confirms an extraordinary CUL morphology in both systems at compositions where an orthorhombic *Fddd* single network appears in the linear ABC counterparts. The replacement of the *Fddd* network by the CUL is attributed to the stiff bottlebrush architecture, which hinders interaction between the network domain and the matrix domain. Furthermore, the compositional dispersity effect on the phase behavior of block bottlebrushes was investigated by fractionation with automated liquid chromatography. A

distribution of morphologies, including the CUL phase, emerged from the polymer fractions obtained from the assynthesized "narrow" parent bottlebrush. These results highlight the importance of accounting for macromolecular dispersity and demonstrate the feasibility of dissecting ABC bottlebrush specimens into offspring morphologies. The identification of the CUL in ABC bottlebrush block terpolymers signifies a promising avenue for leveraging rigid bottlebrush architectures to create novel materials and should inspire additional investigation into the phase behavior of this new class of block polymers.

ASSOCIATED CONTENT

Solution Supporting Information

The Supporting Information is available free of charge at https://pubs.acs.org/doi/10.1021/jacs.3c13543.

Detailed synthesized route; ¹H NMR spectra; SEC traces; molecular parameters; differential scanning calorimetry (DSC) traces; SAXS patterns; TEM images; phase portraits; TLC results; and separation curve from automated liquid chromatography (PDF)

ET reconstruction map (MP4)

AUTHOR INFORMATION

Corresponding Authors

Frank S. Bates – Department of Chemical Engineering & Materials Science, University of Minnesota, Minneapolis, Minnesota 55455, United States; oorcid.org/0000-0003-3977-1278; Email: bates001@umn.edu

Timothy P. Lodge — Department of Chemistry and Department of Chemical Engineering & Materials Science, University of Minnesota, Minneapolis, Minnesota 55455, United States; orcid.org/0000-0001-5916-8834; Email: lodge@umn.edu

Authors

Shuquan Cui — Department of Chemistry, University of Minnesota, Minneapolis, Minnesota 55455, United States Elizabeth A. Murphy — Materials Research Laboratory and Department of Chemistry & Biochemistry, University of California, Santa Barbara, California 93106, United States; orcid.org/0000-0003-0846-7943

Wei Zhang – Department of Diagnostic and Biological Sciences, School of Dentistry, Institute for Molecular Virology and Characterization Facility, College of Science and Engineering, University of Minnesota, Minneapolis, Minnesota 55455, United States

Aristotelis Zografos — Department of Chemical Engineering & Materials Science, University of Minnesota, Minneapolis, Minnesota 55455, United States; orcid.org/0000-0001-9612-091X

Liyang Shen — Department of Chemical Engineering & Materials Science, University of Minnesota, Minneapolis, Minnesota 55455, United States; orcid.org/0000-0001-9928-2877

Complete contact information is available at: https://pubs.acs.org/10.1021/jacs.3c13543

Notes

The authors declare no competing financial interest.

ACKNOWLEDGMENTS

This work was supported by the National Science Foundation (NSF) through the University of Minnesota MRSEC under Award DMR-2011401. Parts of this work were carried out in the Characterization Facility, University of Minnesota, which receives partial support from NSF through the MRSEC program. The research reported here was partially supported by the BioPACIFIC Materials Innovation Platform of the National Science Foundation under Award No. DMR-1933487 (equipment and characterization). Synchrotron SAXS experiments were performed at the 5-ID-D beamlines of the Advanced Photon Source (APS). This research used resources of the Advanced Photon Source, a U.S. Department of Energy (DOE) Office of Science User Facility operated for the DOE Office of Science by Argonne National Laboratory under contract No. DE-AC02-06CH11357. The authors thank Prof. Andre Mkhoyan for fruitful discussions on electron tomography, Dr. Fang Zhou for the help in cryo-microtoming and ET sample preparation, and Pengyu Chen for discussions on morphology identification.

REFERENCES

- (1) Kumar, S.; Bhushan, P.; Bhattacharya, S.; Bhattacharya, S.; Agarwal, A. K.; Chanda, N.; Pandey, A.; Sen, A. K. Fabrication of Nanostructures with Bottom-Up Approach and Their Utility in Diagnostics, Therapeutics, and Others. In *Environmental, Chemical and Medical Sensors*; Springer Singapore: Singapore, 2018; pp 167–198
- (2) Zhang, J. L.; Yu, X. H.; Yang, P.; Peng, J.; Luo, C. X.; Huang, W. H.; Han, Y. C. Microphase Separation of Block Copolymer Thin Films. *Macromol. Rapid Commun.* **2010**, 31, 591–608.
- (3) Steube, M.; Johann, T.; Barent, R. D.; Mueller, A. H. E.; Frey, H. Rational Design of Tapered Multiblock Copolymers for Thermoplastic Elastomers. *Prog. Polym. Sci.* **2022**, *124*, No. 101488.
- (4) Robertson, M.; Guillen-Obando, A.; Barbour, A.; Smith, P.; Griffin, A.; Qiang, Z. Direct Synthesis of Ordered Mesoporous Materials from Thermoplastic Elastomers. *Nat. Commun.* **2023**, *14*, No. 639.
- (5) Zhao, D. Y.; Feng, J. L.; Huo, Q. S.; Melosh, N.; Fredrickson, G. H.; Chmelka, B. F.; Stucky, G. D. Triblock Copolymer Syntheses of Mesoporous Silica with Periodic 50 to 300 Angstrom Pores. *Science* 1998, 279, 548–552.
- (6) Malenfant, P. R. L.; Wan, J. L.; Taylor, S. T.; Manoharan, M. Self-Assembly of An Organic-Inorganic Block Copolymer for Nano-Ordered Ceramics. *Nat. Nanotechnol.* **2007**, *2*, 43–46.
- (7) Tang, C. B.; Lennon, E. M.; Fredrickson, G. H.; Kramer, E. J.; Hawker, C. J. Evolution of Block Copolymer Lithography to Highly Ordered Square Arrays. *Science* **2008**, 322, 429–432.
- (8) Tan, K. W.; Jung, B.; Werner, J. G.; Rhoades, E. R.; Thompson, M. O.; Wiesner, U. Transient Laser Heating Induced Hierarchical Porous Structures from Block Copolymer-Directed Self-Assembly. *Science* 2015, 349, 54–58.
- (9) Kim, H. C.; Park, S. M.; Hinsberg, W. D. Block Copolymer Based Nanostructures: Materials, Processes, and Applications to Electronics. *Chem. Rev.* **2010**, *110*, 146–177.
- (10) Bates, F. S. Polymer-Polymer Phase-Behavior. Science 1991, 251, 898-905.
- (11) Bates, C. M.; Bates, F. S. 50th Anniversary Perspective: Block Polymers Pure Potential. *Macromolecules* **2017**, *50*, 3–22.
- (12) Leibler, L. Theory of Microphase Separation in Block Co-Polymers. *Macromolecules* **1980**, *13*, 1602–1617.
- (13) Lodge, T. P. Block Copolymers: Long-Term Growth with Added Value. *Macromolecules* **2020**, *53*, 2–4.
- (14) Bates, F. S.; Fredrickson, G. H. Block Copolymers Designer Soft Materials. *Phys. Today* **1999**, *52*, 32–38.

- (15) Bates, F. S.; Hillmyer, M. A.; Lodge, T. P.; Bates, C. M.; Delaney, K. T.; Fredrickson, G. H. Multiblock Polymers: Panacea or Pandora's Box? *Science* **2012**, *336*, 434–440.
- (16) Chang, A. B.; Bates, F. S. The ABCs of Block Polymers. *Macromolecules* **2020**, 53, 2765–2768.
- (17) Verduzco, R.; Li, X. Y.; Peseka, S. L.; Steinc, G. E. Structure, Function, Self-assembly, and Applications of Bottlebrush Copolymers. *Chem. Soc. Rev.* **2015**, *44*, 2405–2420.
- (18) Li, Z. L.; Tang, M.; Liang, S.; Zhang, M. Y.; Biesold, G. M.; He, Y. J.; Hao, S. M.; Choi, W.; Liu, Y. J.; Peng, J.; Lin, Z. Q. Bottlebrush Polymers: From Controlled Synthesis, Self-Assembly, Properties to Applications. *Prog. Polym. Sci.* **2021**, *116*, No. 101387.
- (19) Paturej, J.; Sheiko, S. S.; Panyukov, S.; Rubinstein, M. Molecular Structure of Bottlebrush Polymers in Melts. *Sci. Adv.* **2016**, 2, No. e1601478.
- (20) Rzayev, J. Synthesis of Polystyrene-Polylactide Bottlebrush Block Copolymers and Their Melt Self-Assembly into Large Domain Nanostructures. *Macromolecules* **2009**, *42*, 2135–2141.
- (21) Sveinbjörnsson, B. R.; Weitekamp, R. A.; Miyake, G. M.; Xia, Y.; Atwater, H. A.; Grubbs, R. H. Rapid Self-Assembly of Brush Block Copolymers to Photonic Crystals. *Proc. Natl. Acad. Sci. U.S.A.* **2012**, 109, 14332–14336.
- (22) Miyake, G. M.; Weitekamp, R. A.; Piunova, V. A.; Grubbs, R. H. Synthesis of Isocyanate-Based Brush Block Copolymers and Their Rapid Self-Assembly to Infrared-Reflecting Photonic Crystals. *J. Am. Chem. Soc.* **2012**, *134*, 14249–14254.
- (23) Macfarlane, R. J.; Kim, B.; Lee, B.; Weitekamp, R. A.; Bates, C. M.; Lee, S. F.; Chang, A. B.; Delaney, K. T.; Fredrickson, G. H.; Atwater, H. A.; Grubbs, R. H. Improving Brush Polymer Infrared One-Dimensional Photonic Crystals via Linear Polymer Additives. J. Am. Chem. Soc. 2014, 136, 17374—17377.
- (24) Park, S. J.; Cheong, G. K.; Bates, F. S.; Dorfman, K. D. Stability of the Double Gyroid Phase in Bottlebrush Diblock Copolymer Melts. *Macromolecules* **2021**, *54*, 9063–9070.
- (25) Gai, Y.; Song, D. P.; Yavitt, B. M.; Watkins, J. J. Polystyrene-block-Poly(ethylene oxide) Bottlebrush Block Copolymer Morphology Transitions: Influence of Side Chain Length and Volume Fraction. *Macromolecules* **2017**, *50*, 1503–1511.
- (26) Jiang, L. Y.; Nykypanchuk, D.; Pastore, V. J.; Rzayev, J. Morphological Behavior of Compositionally Gradient Polystyrene-Polylactide Bottlebrush Copolymers. *Macromolecules* **2019**, *52*, 8217–8226.
- (27) Matsen, M. W.; Bates, F. S. Origins of Complex Self-Assembly in Block Copolymers. *Macromolecules* **1996**, *29*, 7641–7644.
- (28) Kawamoto, K.; Zhong, M. J.; Gadelrab, K. R.; Cheng, L. C.; Ross, C. A.; Alexander-Katz, A.; Johnson, J. A. Graft-through Synthesis and Assembly of Janus Bottlebrush Polymers from A-Branch-B Diblock Macromonomers. J. Am. Chem. Soc. 2016, 138, 11501–11504.
- (29) Liang, R. Q.; Xue, Y. Z.; Fu, X. W.; Le, A. N.; Song, Q. L.; Qiang, Y. C.; Xie, Q.; Dong, R. Q.; Sun, Z. H.; Osuji, C. O.; Johnson, J. A.; Li, W. H.; Zhong, M. J. Hierarchically Engineered Nanostructures from Compositionally Anisotropic Molecular Building Blocks. *Nat. Mater.* **2022**, *21*, 1434–1440.
- (30) Sun, Z. H.; Liu, R. Z.; Su, T. Y.; Huang, H. J.; Kawamoto, K.; Liang, R. Q.; Liu, B.; Zhong, M. J.; Alexander-Katz, A.; Ross, C. A.; Johnson, J. A. Emergence of Layered Nanoscale Mesh Networks through Intrinsic Molecular Confinement Self-assembly. *Nat. Nanotechnol.* **2023**, *18*, 273–280.
- (31) Cui, S. Q.; Zhang, B.; Shen, L. Y.; Bates, F. S.; Lodge, T. P. Core-Shell Gyroid in ABC Bottlebrush Block Terpolymers. *J. Am. Chem. Soc.* **2022**, 144, 21719–21727.
- (32) Epps, T. H.; Cochran, E. W.; Bailey, T. S.; Waletzko, R. S.; Hardy, C. M.; Bates, F. S. Ordered Network Phases in Linear Poly(isoprene-b-styrene-b-ethylene oxide) Triblock Copolymers. *Macromolecules* **2004**, *37*, 8325–8341.
- (33) Tyler, C. A.; Morse, D. C. Orthorhombic Fddd Network in Triblock and Diblock Copolymer Melts. *Phys. Rev. Lett.* **2005**, 94, No. 208302.

- (34) Chang, A. B.; Bates, F. S. Impact of Architectural Asymmetry on Frank-Kasper Phase Formation in Block Polymer Melts. *ACS Nano* **2020**, *14*, 11463–11472.
- (35) Schmidt, S. C.; Hillmyer, M. A. Morphological Behavior of Model Poly(ethylene-alt-propylene)-b-Polylactide Diblock Copolymers. J. Polym. Sci., Part B: Polym. Phys. 2002, 40, 2364–2376.
- (36) Lindsay, A. P.; Jayaraman, A.; Peterson, A. J.; Mueller, A. J.; Weigand, S.; Almdal, K.; Mahanthappa, M. K.; Lodge, T. P.; Bates, F. S. Reevaluation of Poly(ethylene-alt-propylene)-block-Polydimethylsiloxane Phase Behavior Uncovers Topological Close-Packing and Epitaxial Quasicrystal Growth. ACS Nano 2021, 15, 9453–9468.
- (37) Lee, S.; Bluemle, M. J.; Bates, F. S. Discovery of a Frank-Kasper σ Phase in Sphere-Forming Block Copolymer Melts. *Science* **2010**, 330, 349–353.
- (38) Ercius, P.; Alaidi, O.; Rames, M. J.; Ren, G. Electron Tomography: A Three-Dimensional Analytic Tool for Hard and Soft Materials Research. *Adv. Mater.* **2015**, 27, 5638–5663.
- (39) Kremer, J. R.; Mastronarde, D. N.; McIntosh, J. R. Computer Visualization of Three-Dimensional Image Data Using IMOD. *J. Struct. Biol.* **1996**, *116*, 71–76.
- (40) Scaramuzza, S.; Castano-Diez, D. Step-by-Step Guide to Efficient Subtomogram Averaging of Virus-Like Particles with Dynamo. *PLoS Biol.* **2021**, *19*, No. e3001318.
- (41) Xie, S. Y.; Lodge, T. P. Phase Behavior of Binary Polymer Blends Doped with Salt. *Macromolecules* **2018**, *51*, 266–274.
- (42) Lynd, N. A.; Hillmyer, M. A. Influence of Polydispersity on the Self-Assembly of Diblock Copolymers. *Macromolecules* **2005**, *38*, 8803–8810.
- (43) Oschmann, B.; Lawrence, J.; Schulze, M. W.; Ren, J. M.; Anastasaki, A.; Luo, Y. D.; Nothling, M. D.; Pester, C. W.; Delaney, K. T.; Connal, L. A.; McGrath, A. J.; Clark, P. G.; Bates, C. M.; Hawker, C. J. Effects of Tailored Dispersity on the Self-Assembly of Dimethylsiloxane-Methyl Methacrylate Block Co-Oligomers. *ACS Macro Lett.* **2017**, *6*, 668–673.
- (44) Schmitt, A. K.; Mahanthappa, M. K. Order and Disorder in High χ /Low N, Broad Dispersity ABA Triblock Polymers. *Macromolecules* **2017**, *50*, *6779*–*6787*.
- (45) Sun, Y. X.; Tan, R.; Ma, Z.; Gan, Z. H.; Li, G.; Zhou, D. D.; Shao, Y.; Zhang, W. B.; Zhang, R.; Dong, X. H. Discrete Block Copolymers with Diverse Architectures: Resolving Complex Spherical Phases with One Monomer Resolution. *ACS Cent. Sci.* **2020**, *6*, 1386–1393.
- (46) Lin, T. P.; Chang, A. B.; Chen, H. Y.; Liberman-Martin, A. L.; Bates, C. M.; Voegtle, M. J.; Bauer, C. A.; Grubbs, R. H. Control of Grafting Density and Distribution in Graft Polymers by Living Ring-Opening Metathesis Copolymerization. *J. Am. Chem. Soc.* **2017**, *139*, 3896–3903.
- (47) Chang, A. B.; Lin, T. P.; Thompson, N. B.; Luo, S. X.; Liberman-Martin, A. L.; Chen, H. Y.; Lee, B.; Grubbs, R. H. Design, Synthesis, and Self-Assembly of Polymers with Tailored Graft Distributions. *J. Am. Chem. Soc.* **2017**, *139*, 17683–17693.
- (48) Park, S.; Cho, D.; Ryu, J.; Kwon, K.; Lee, W.; Chang, T. Fractionation of Block Copolymers Prepared by Anionic Polymerization into Fractions Exhibiting Three Different Morphologies. *Macromolecules* **2002**, *35*, 5974–5979.
- (49) Lee, S.; Lee, H.; Chang, T.; Hirao, A. Synthesis and Characterization of an Exact Polystyrene-graft-polyisoprene: A Failure of Size Exclusion Chromatography Analysis. *Macromolecules* **2017**, *50*, 2768–2776.
- (50) Zhang, C.; Bates, M. W.; Geng, Z. S.; Levi, A. E.; Vigil, D.; Barbon, S. M.; Loman, T.; Delaney, K. T.; Fredrickson, G. H.; Bates, C. M.; Whittaker, A. K.; Hawker, C. J. Rapid Generation of Block Copolymer Libraries Using Automated Chromatographic Separation. *J. Am. Chem. Soc.* **2020**, *142*, 9843–9849.
- (51) Murphy, E. A.; Chen, Y. Q.; Albanese, K.; Blankenship, J. R.; Abdilla, A.; Bates, M. W.; Zhang, C.; Bates, C. M.; Hawker, C. J. Efficient Creation and Morphological Analysis of ABC Triblock Terpolymer Libraries. *Macromolecules* **2022**, *55*, 8875–8882.

- (52) Löbling, T. I.; Hiekkataipale, P.; Hanisch, A.; Bennet, F.; Schmalz, H.; Ikkala, O.; Groeschel, A. H.; Muller, A. H. E. Bulk Morphologies of Polystyrene-block-Polybutadiene-block-Poly(tertbutyl methacrylate) Triblock Terpolymers. *Polymer* **2015**, *72*, 479–489
- (53) Jiang, S. M.; Gopfert, A.; Abetz, V. Novel Morphologies of Block Copolymer Blends via Hydrogen Bonding. *Macromolecules* **2003**, *36*, 6171–6177.
- (54) Sakurai, S.; Hashimoto, T.; Fetters, L. J. Morphology of Polystyrene-block-Poly(ethylene-alt-propylene) Diblock Copolymers in the Strong-Segregation Limit. *Macromolecules* **1995**, 28, 7947–7949
- (55) Sinturel, C.; Bates, F. S.; Hillmyer, M. A. High χ -Low N Block Polymers: How Far Can We Go? *ACS Macro Lett.* **2015**, *4*, 1044–1050
- (56) Cochran, E. W.; Morse, D. C.; Bates, F. S. Design of ABC Triblock Copolymers near the ODT with the Random Phase Approximation. *Macromolecules* **2003**, 36, 782–792.
- (\$7) Meuler, A. J.; Hillmyer, M. A.; Bates, F. S. Ordered Network Mesostructures in Block Polymer Materials. *Macromolecules* **2009**, *42*, 7221–7250.
- (58) Tyler, C. A.; Qin, J.; Bates, F. S.; Morse, D. C. SCFT Study of Nonfrustrated ABC Triblock Copolymer Melts. *Macromolecules* **2007**, 40, 4654–4668.
- (59) Matsen, M. W.; Beardsley, T. M.; Willis, J. D. Fluctuation-Corrected Phase Diagrams for Diblock Copolymer Melts. *Phys. Rev. Lett.* **2023**, *130*, No. 248101.
- (60) Zhang, B.; Cui, S. Q.; Lodge, T. P.; Bates, F. S. Structure and Phase Behavior of Bottlebrush Diblock Copolymer-Linear Homopolymer Ternary Blends. *Macromolecules* **2023**, *56*, 1663–1673.
- (61) Matsen, M. W.; Bates, F. S. Block Copolymer Microstructures in the Intermediate-Segregation Regime. *J. Chem. Phys.* **1997**, *106*, 2436–2448.